Matrix Infrared Spectroscopic Study of Magnesium Carbene and Carbenoid Radicals and Analysis of Their Bonding with Density Functional Calculations

William D. Bare, Angelo Citra, Carl Trindle, and Lester Andrews*

Department of Chemistry, University of Virginia, McCormick Road, Charlottesville, Virginia 22901

Received October 19, 1999

Magnesium atoms generated by laser ablation were reacted with methyl halides and methane diluted in argon. Among the reaction products were the metal carbene species, $MgCH_2$, and carbenoid radicals, $XMgCH_2$ (where X = H, F, C1, and Br). This investigation reports matrix infrared spectra for Mg carbene and carbenoid species in a cold matrix, and electronic structure calculations for these and related beryllium species. An unusual bonding interaction for the MCH_2 species is described in which the bonding in the α and β manifolds is qualitatively different. Vibrational frequencies and analysis of the results of density functional calculations provide information about the nature of the bonding in these species and allow for a comparison to the well-known transition metal Fischer- and Schrock-type carbene complexes. The special difficulties of computational modeling of vibrations in highly polar molecules are discussed.

Introduction

The current study was prompted by previous investigations of the reactions of laser-ablated magnesium and beryllium atoms with methane and methyl halides undertaken primarily to investigate the formation and infrared spectra of CH_3MX molecules.[1,2] Although the CH_3MX molecules were produced in these reactions, several halogen-independent bands were also observed in each system. These bands could not be assigned to CH_3MH and indicated the presence of smaller MCH_n fragments. This result provoked great interest in our laboratory regarding the formation of group II metal carbenes and related species by laser ablation. Transition metal (Fe and Cu) carbene complexes resulting from the reaction of thermally evaporated metal atoms with diazomethane (CH_2N_2) have previously been observed in argon matrixes;[3,4] however, infrared spectra of group II metal carbene complexes and carbenoid radicals have not previously been reported.

The group II metal carbene complexes, $BeCH_2$ and $MgCH_2$, and related species have been the subject of much investigation by theoretical chemists over the past two decades.[5−10] There are two reasons for such intense interest in these molecules. First, the structure of these species is such that they may be expected to contain a formal double bond between carbon and a group II metal atom. Bonding of this type is quite unusual, and the possibility of Be═C and Mg═C bonding has been a major driving force for previous theoretical investigations. Second, these species represent very simple analogues of the well-known Fischer and Schrock carbenes and provide an interesting comparison with respect to bonding and electronic structure.[11]

Scheme 1

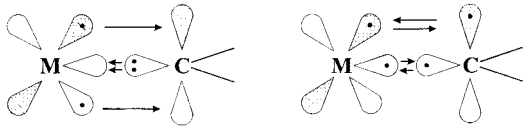

1 Fischer-type Carbene Complex **2** Schrock-type Carbene Complex

Two bonding schemes for metal carbene complexes have been described by Taylor and Hall[12] in which the bonding is most conveniently understood as occurring between a metal atom and a carbene fragment. The most important orbitals for bonding of carbene fragments (CRR′) are an a_1 (carbon sp^2) and a slightly higher b_1 (carbon p) orbital, which may be variously occupied to give either a singlet or triplet depending upon the nature of the groups R and R′. When R and R′ are both H (i.e., CH_2), the ground state is a triplet.

The metal−carbon bond in a Fischer-type carbene can be described as a dative bond from the doubly occupied a_1 orbital of a singlet carbene fragment with some stabilizing π back-bonding from metal d orbitals to the empty b_1 orbital of methylene, much like the metal−carbon bond of a metal carbonyl complex. (See **1** in Scheme 1.) Fischer-type carbene complexes are favored by metals with low oxidation states and by singlet carbene fragments. Schrock-type carbene complexes, favored by high-valent metals and by triplet carbene fragments, can be considered to have a σ and π bond resulting from overlap of singly occupied orbitals on the metal and the carbene, roughly analogous to the bonding in ethene, as in Scheme 1, **2**. These

(1) Greene, T. M.; Lanzisera, D. V.; Andrews, L.; Downs, A. J. *J. Am. Chem. Soc.* **1998**, *120*, 6097.
(2) Bare, W. D.; Andrews, L. *J. Am. Chem. Soc.* **1998**, *120*, 7293.
(3) Sou-Chan, C.; Kafafi, Z. H.; Hauge, R. H.; Billups, W. E.; Margrave, J. L. *J. Am. Chem. Soc.* **1985**, *107*, 1447. Sou-Chan, C.; Hauge, R. H.; Kafafi, Z. H.; Margrave, J. L.; Billups, W. E. *J. Am. Chem. Soc.* **1988**, *110*, 7975.
(4) Sou-Chan, C.; Kafafi, Z. H.; Hauge, R. H.; Billups, W. E.; Margrave, J. L. *J. Am. Chem. Soc.* **1987**, *109*, 4508.
(5) Dill, J. D.; Schleyer, P. v. R.; Binkley, J. S.; Pople, J. A. *J. Am. Chem. Soc.* **1977**, *99*, 6159.
(6) Binkley, J. S.; Seeger, R.; Pople, J. A.; Dill, J. D.; Schleyer, P. v. R. *Theor. Chim. Acta* **1977**, *45*, 69.
(7) Luke, B. T.; Pople, J. A.; Schleyer, P. v. R. *Chem. Phys. Lett.* **1983**, *97*, 265.
(8) Luke, B. T.; Pople, J. A.; Krogh-Jespersen, M.; Apeloig, Y.; Karni, M.; Chandrasekhar, J.; Schleyer, P. v. R. *J. Am. Chem. Soc.* **1986**, *108*, 270.
(9) Sana, M.; Leroy, G. *Theor. Chim. Acta* **1990**, *77*, 383.
(10) Sunil, K. K. *J. Phys. Chem.* **1993**, *99*, 7553.
(11) Crabtree, R. H. *Organometallic Chemistry of the Transition Metals*, 2nd ed.; Wiley: New York, 1994.
(12) Taylor, T. E.; Hall, M. B. *J Am. Chem. Soc.* **1984**, *106*, 1576.

10.1021/ic991229m CCC: $19.00
Published on Web 03/02/2000

Table 1. Calculated (DFT/B3LYP) Electronic Configurations, Energies (kcal/mol), Be−C Bond Energies, and Vibrational Frequencies (cm^{-1}) for $BeCH_2$ Carbene and Related $XBeCH_2$ Carbenoid Radicals

molecule	electronic state	total bonding energy (kcal/mol)	Be−C bond energy (kcal/mol)	frequencies (cm^{-1}), symmetries, and intensities (km/mol) of normal modes		
$BeCH_2$	$^1A'$	243	54	572.5, a″, 95;	591.5, a′, 145;	962.9, a′, 193;
				1375.5, a′, 9;	3061.2, a′, 9;	3130.4, a″, 2
$BeCH_2$	$^3B_1$	260	71	544.8, b_2, 1;	684.3, b_1, 60;	951.6, a_1, 56;
				1406.7, a_1, 18;	3071.5, a_1, 8;	3140.0, b_2, 6
$HBeCH_2$	$^2B_1$	356	110	435.5, b_2, 37;	533.2, b_1, 61;	686.3, b_1, 163;
				717.2, b_2, 195;	941.3, a_1, 39;	1421.5, a_1, 19;
				2158.6, a_1, 194;	3082.0, a_1, 3;	3144.6, b_2, 9
$FBeCH_2$	$^2B_1$	431	106	270.4, b_2, 35;	317.0, b_1, 44;	647.4, b_1, 101;
				648.3, a_1, 1;	673.9, b_2, 102;	1380.4, a_1, 179;
				1427.9, a_1, 124;	3096.9, a_1, 3;	3164.9, b_2, 7
$ClBeCH_2$	$^2B_1$	391	108	227.3, b_2, 17;	263.5, b_1, 20;	504.6, a_1, 10;
				660.3, b_1, 82;	660.5, b_2, 67;	1181.5, a_1, 284;
				1421.0, a_1, 29;	3093.1, a_1, 3;	3159.8, b_2, 6
$BrBeCH_2$	$^2B_1$	376	107	210.7, b_2, 12;	241.3, b_1, 14;	422.6, a_1, 11;
				653.5, b_2, 57;	663.2, b_1, 77;	1137.8, a_1, 262;
				1420.8, a_1, 26;	3091.8, b_2, 3;	3157.9, b_2, 6

two bonding schemes give rise to different characteristic chemical reactivities for the resulting metal carbene species. The largely unoccupied b_1 (carbon p) orbital of Fischer carbene complexes leads these species to behave as electrophiles, while Schrock-type carbene complexes, with an electron-rich double bond, behave as nucleophiles.

The well-known importance of the metal−carbon bonding scheme in metal carbene complexes and its effect on reactivity has provoked a question: *"Can the p orbitals of group II metals participate in bonding to carbene fragments to produce metal−carbon double-bond character, and if so, can this bonding be more accurately described as the Fischer or Schrock type?"* To address these questions we present infrared spectra of the magnesium carbene complex ($MgCH_2$) and related carbenoid radical ($XMgCH_2$) species isolated in a cryogenic argon matrix, and theoretical representations of the bonding in these systems.

Experimental Section

The apparatus used for laser ablation and matrix isolation of products has been described previously.[13,14] Methane, methyl fluoride, methyl chloride, and methyl bromide (all from Matheson) samples were used as received and diluted with argon (Airco) to yield 1:200 or 1:400 (CH_3X:Ar) mixtures. Diluted methane samples were passed through a Dewar of liquid nitrogen to remove impurities. A magnesium (Fisher) disk mounted on a rotating (1 rpm) rod was ablated by a focused Nd:YAG laser (1064 nm) with a pulse rate of 10 Hz and with energy of 10−20 mJ/pulse. Gas mixtures were deposited on a 10 ± 1 K CsI window at a rate of 2 mmol/h for 1−2 h with concurrent ablation of the magnesium target. Infrared spectra were recorded using a Nicolet 750 Fourier transform infrared spectrophotometer with 0.5 cm^{-1} resolution. After initial spectra were recorded, the matrixes were subjected to stepwise annealing to 25, 30, and 35 K, with spectra recorded after each cycle. Matrixes were also subjected to 240−580 nm photolysis from a medium-pressure Hg arc lamp (Philips 175W with glass globe removed). Spectra were recorded after photolysis. Experiments were repeated using isotopically enriched samples, including ^{26}Mg (Oak Ridge National Laboratory, 95% ^{26}Mg), CD_3Br and CD_4 (MSD Isotopes), CD_3F (prepared as described previously[15]), $^{13}CH_3F$, and $^{13}CH_4$ (MSD Isotopes).

Calculational Methods

The method of choice for structure, energetics, and vibrational force field for molecules of moderate size is density functional theory (DFT). We supplemented DFT methods with MP2 and CASSCF calculations for occasional checks and alternative viewpoints. In all calculations we used the Gaussian94 program[16] operating on an SP2 computer and the G98W code on several Windows/Intel work stations.

We used two gradient-corrected versions of DFT, the B3LYP and BP86 functionals. Our experience is that B3LYP calculations generally provide more accurate calculations of molecular energy[17] while BP86 calculations often provide a better mimic of observed anharmonic frequencies.[15] We routinely used a flexible basis set including diffuse and polarization functions, called 6-311+G*, except in occasional checks. We supplemented the Mulliken populations reported in the usual output with the more reliable natural bond order (NBO) charges for all carbene and carbenoid complexes.

Summary of Computations: Structure and Bonding

The computational survey of energies, vibrational frequencies and absorption intensities for Mg and Be methylene species, with isotopic variants, is summarized in Tables 1 and 2, and geometries are presented in Figure 1. Total bonding energies presented here are the difference between the calculated energy of the molecule and the sum of calculated energies of its constituent atoms as determined with the same method and basis set. Likewise, M−C bond energies are the difference between the calculated molecular energy and the sum of the energies of the XM and CH_2 fragments. In the discussion of the performance of these calculations, it will be necessary to refer to calculations of similar known species with highly ionic metal−carbon bonds. For this reason, calculations have also been performed on $MgCH_3$, $LiCH_3$, $NaCH_3$, and KCH_3, for which results are collected in Table 3.

In our survey calculations on $X-M-CH_2$ species, we imposed no symmetry constraints. While the MCH_2 singlet assumed a C_s (pyramidal) form, the triplet MCH_2 and all doublet $XMCH_2$ systems converged to C_{2v} symmetry. In subsequent calculations, C_{2v} symmetry was imposed for these molecules by defining X−M−C bond angles and appropriate dihedral angles as 180.0°. In describing the geometry of all C_{2v} species,

(13) Burkholder, T. R.; Andrews, L. J. *Chem. Phys.* **1991**, *95*, 8679. Hassenzadeh, P.; Andrews, L. *J. Phys. Chem.* **1992**, *96*, 9177.
(14) Lanzisera, D. V.; Andrews L. *J. Am. Chem. Soc.* **1997**, *119*, 6392.
(15) Andrews, L.; Dyke, J. M.; Jonathan, N.; Keddar, N.; Morris, A.; Ridha, A. *J. Phys. Chem.* **1984**, *88*, 2364.
(16) Frisch, M. J.; Trucks, G. W.; Schlegel, H. B.; Gill, P. M. W.; Johnson, B. G.; Robb, M. A.; Cheeseman, J. R.; Keith. T.; Petersson, G. A.; Montgomery, J. A.;. Raghavachari, K.; Al-Laham, M. A.; Zakrzewski, V. G.; Ortiz, J. V.; Foresman, J. B.; Cioslowski, J.: Steianov, B. B.; Nanayakkara, A.; Challacombe, M.; Peng, C. Y.; Ayala, P. Y.; Chen, W.; Wong, M. W.; Andres, J. L.; Replogle, E. S.; Gomperts, R.; Martin, R. L.; Fox, D. J.; Binkley, J. S.; Defrees, D. J.; Baker, J.; Stewart, J. P.; Head-Gordon, M.; Gonzalez, C.; Pople, J. A. *Gaussian 94*, Revision B.1; Gaussian, Inc.: Pittsburgh, PA, 1995.
(17) Scott, A. P.; Radom, L. J. *Phys. Chem.* **1996**, *100*, 16502.

Table 2. Calculated (DFT/B3LYP) Electronic Configurations, Bond Energies, and Vibrational Frequencies and Intensities for $MgCH_2$ Carbene and Related $XMgCH_2$ Carbenoid Radicals

molecule	electronic state	total bonding energy (kcal/mol)	Be−C bond energy (kcal/mol)	frequencies (cm^{-1}), symmetries, and intensities (km/mol) of normal modes		
$MgCH_2$	$^1A'$	215	26	478.0, a′, 44; 1401.3, a′, 19;	569.4, a″, 53; 2928.0, a′, 52;	661.3, a′, 349; 2993.8, a″, 26
$MgCH_2$	$^3B_1$	226	37	458.5, b_2, 5; 1357.6, a_1, 21;	537.2, a_1, 39; 3032.6, a_1, 72;	607.6, b_1, 89; 3115.1, b_2, 20
$Mg^{13}CH_2$	$^3B_1$	226	37	456.0, b_2; 1352.6, a_1;	525.7, a_1; 3027.1, a_1;	602.4, b_1; 3103.3, b_2
$^{26}MgCH_2$	$^3B_1$	226	37	458.1, b_2; 1357.5, a_1;	529.5, a_1; 3032.6, a_1;	607.4, b_1; 3115.1, b_2
$MgCD_2$	$^3B_1$	226	37	347.0, b_2; 1005.8, a_1;	475.7, b_1; 2196.5, a_1;	514.0, a_1; 2309.8, b_2
$HMgCH_2$	$^2B_1$	297	76	314.0, b_2, 167; 564.1, b_1, 110; 1633.5, a_1, 243;	343.6, b_1, 212; 588.9, a_1, 38; 3040.4, a_1, 40;	533.0, b_2, 163; 1397.5, a_1, 4; 3109, b_2, 20
$FMgCH_2$	$^2B_1$	363	75	139.9, b_2, 59; 543.2, b_2, 99; 1390.3, a_1, 2;	149.9, b_1, 65; 554.1, b_1, 86; 3063.2, a_1, 24;	506, a_1, 0.1; 777.3, a_1, 129; 3138.0, b_2, 11
$ClMgCH_2$	$^2B_1$	335	75	121.7, b_2, 36; 540.8, b_2, 81; 119; 1389.9, a_1, 4;	132.1, b_1, 39; 556.5, b_1, 80; 3062.1, a_1, 28;	384.1, a_1, 16; 668.6, a_1; 3137.1, b_2, 12
$BrMgCH_2$	$^2B_1$	324	74	112.2, b_2, 28; 538.1, b_2, 74; 1389.4, a_1, 6;	121.8, b_1, 31; 555.1, b_1, 78; 3061.0, a_1, 31;	308.7, a_1, 15; 650.1, a_1, 107; 3136.1, b_2, 11

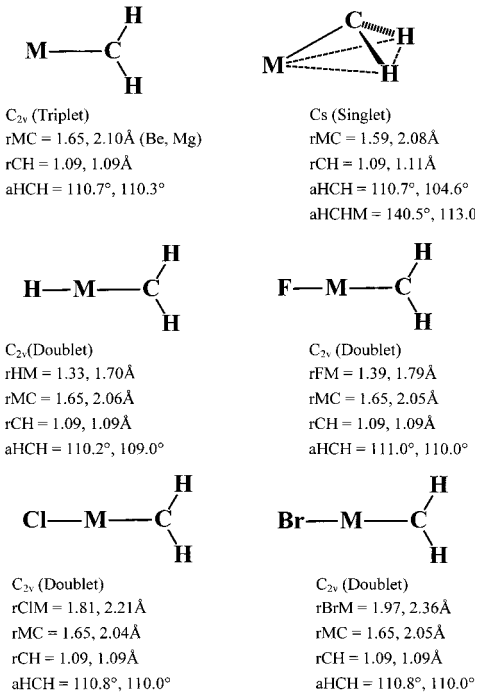

Figure 1. Calculated (B3LYP/6-311+G*) structures for beryllium and magnesium carbene and carbenoid species. Two numbers are given for each geometric parameter, which correspond to the Be and Mg species, respectively.

the following designations are employed: The molecules lie in the *yz* plane with the metal−carbon axis along the *z*-axis (a_1). The π-bonding orbitals (b_1) are parallel to the *x*-axis, and the pseudo-π orbitals (b_2) are parallel to the *y*-axis. All $M-CH_3$ species were described within C_{3v} symmetry. Due to the unusual nature of many of these molecules, we supplemented results obtained from DFT with MP2 calculations for several of these species. In all cases, MP2, DFT/BP86, and DFT/B3LYP all gave quantitatively similar and qualitatively identical results. Presented here are the results of unrestricted DFT/B3LYP calculations, with orbital occupations and charge delocalization from NBO analyses.

Singlet MCH_2. The metal carbene can exist in a singlet or triplet state. The first question to consider in the discussion of the $MgCH_2$ and $BeCH_2$ molecules is the ground state multiplicity, since these species may reasonably be expected to exist as either a singlet or triplet. Of these, the singlet is perhaps the more interesting, since it is the state most likely to show metal−carbon double-bond character. All calculations performed here as well as previously[5−10] have shown the singlet states to be less stable than the triplet states by 7−12 kcal/mol, indicating that, at 10 K, formation of the singlet molecule is unlikely. The calculated properties of the singlet state are nevertheless of interest insofar as they pertain to metal−carbon bonding.

The pyramidal form of the singlet MCH_2 species argues immediately against a representation of the bonding as $M{=}CH_2$. The deviation from planarity of 39.5° for $BeCH_2$ is substantial, and the 67.0° deviation of $MgCH_2$ is actually very near that of a tetrahedral carbon center (70.5°). A more thorough description of the electronic distribution is provided by the NBO analysis. DFT, CAS, and MP2 calculations all indicated a large degree of charge transfer from metal to carbon (1.098 e^- for $BeCH_2$, and 0.824 e^- for $MgCH_2$, according to DFT/NBO calculation). The result is a highly polarized single σ bond between what is essentially an Mg^+ cation and an sp^3-hybridized CH_2^- anion. The molecule may be thought of as a singlet-coupled diradical.

Triplet MCH_2. DFT and also MP2 methods reveal an unusual bonding picture for the triplet (ground state) MCH_2 species. For these molecules, the α and β electron manifolds contain five and three valence electrons, respectively. One might say that, in the single-determinant spin-unrestricted description, the α electrons inhabit an environment similar to those in the $MgCH_2$ dianion and the β electrons inhabit an environment similar to those in the $MgCH_2$ dication. These differing electronic environments lead to different bonding interactions in each manifold, as shown in Figure 2.

In the α manifold, a weak interaction between the a_1 orbital on the carbene fragment and the metal a_1 (primarily s) orbital results in only a slight mixing and repulsion of orbital energies with no net stabilization. The calculations indicate that these orbitals show very little overlap and are best described as

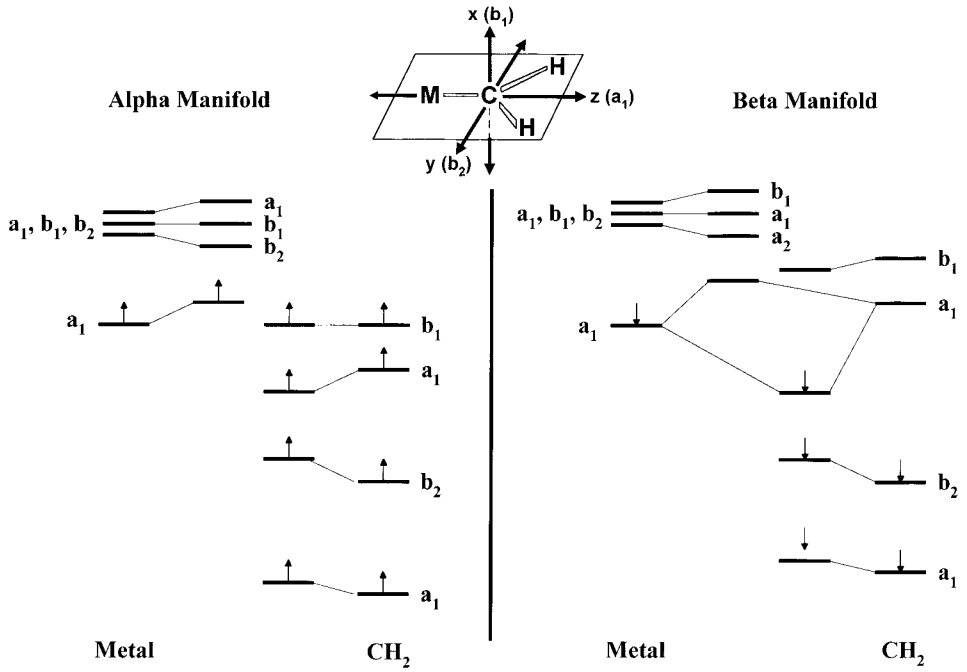

Figure 2. Schematic molecular orbital diagrams for the α and β electron manifolds of $MgCH_2$.

nonbonding orbitals localized on the metal and carbon atoms, respectively. Attending this modest interaction, the electron density about the carbon center is slightly polarized, with a slight decrease in the p character of the nonbonding a_1 orbital and a compensating increase in p character in the bonding a_1 and b_2 orbitals.

In the β manifold, a one-electron bond is formed resulting from electron donation from the metal atom to the a_1 orbital of the carbene fragment. This bond is highly polarized and is NBO-characterized as having 85% and 78% carbon character for the Be and Mg species, respectively. This behavior differs from that of all other X−M−carbenoid radicals (vide infra).

The participation of metal-centered p orbitals in metal−carbon bonding is quite small. For $BeCH_2$, the nonbonding a_1 orbital in the α manifold contains about 7% p character. In the β manifold, for which the metal a_1 orbital bonds with methylene, the Be contribution to the bonding orbital has approximately 11% p character. This does not result in significant *occupation* of the Be p-σ orbital because the bonding electron resides primarily on carbon. The picture is very similar for $MgCH_2$, but the p participation is even less.

We note a small occupation of the metal-centered p-π atomic orbitals in the alkaline earth carbenes (4% for Be, 1% for Mg). These small values derive from electron transfer in the α manifold from carbon to the metal. One may characterize this as π back-bonding, and note that the direction of this electron donation in the σ and π bonds is precisely the *opposite* of that seen in Fischer carbenes. The π donation is, however, much too small to be considered a physically significant feature of the overall bond. The weakness of this π interaction is illustrated by the bond lengths (Be−C = 1.65 Å; Mg−C = 2.10 Å), which are too large to suggest multiple bonding.

We are now in a position to answer the question posed previously, *"Can the p orbitals of group II metals participate in bonding to carbene fragments to produce metal−carbon double-bond character, and if so, can this bonding be more accurately described as the Fischer or Schrock type?"* We must respond, *"Certainly not!"* The triplet is preferred energetically, the singlet is essentially a diradical, and the connection between metal and carbon is best considered of bond order one-half. The bonding cannot be described as either Fischer- or Schrock-like; it is qualitatively quite different from both of these.

$HMCH_2$. The $HMCH_2$ molecules are ground state doublets with C_{2v} geometry. Two dramatic electronic effects are brought about by the addition of a metal-bonded hydrogen atom to the MCH_2 complex. The first is that the charge distributions in the α and β manifolds are more similar (see Figure 3a) and the σ-bonding interaction is qualitatively the same in each (see Figure 3b). The carbon atoms do not rehybridize, maintaining essentially sp^2 character in all three planar orbitals in both electron manifolds. The metal−carbon bond remains highly polarized, but is formed from a bonding orbital containing two electrons, rather than one as was the case with MCH_2. The result of this fundamental change in electronic structure is an increase in metal−methylene bond energy of roughly 40 kcal/mol for both $HBeCH_2$ and $HMgCH_2$.

The second effect is that the metal-centered a_1 orbitals become fully sp hybridized with very nearly 50% s and p character in both a_1 orbitals. This addition of p character to the metal a_1 orbitals allows for more effective overlap with the metal atom's neighbors and also contributes to the strengthening of the metal−carbon bond mentioned above. The increased participation of p orbitals in σ bonding is not reflected in large metal-p amplitude in the molecular orbitals because the bonds are highly polarized away from the metal atoms toward neighbors, so that most of the electron density is assigned in the NBO analysis to the a_1 orbitals of carbon and hydrogen.

There remains a very small π-bonding interaction in the α manifold. As with MCH_2, the minute electron occupation of the metal p-π orbitals is matched by a depletion of electron density on the p-π orbital of carbon. The magnitude of this interaction is very small, not significantly different from that of MCH_2.

$XMCH_2$. All $XMCH_2$ species are ground state doublets with C_{2v} geometry, and the electronic structures of the $XMCH_2$ species resemble those of $HMCH_2$. The metal atoms are sp hybridized and form a polar, two-electron bond with carbon. There is also some occupation of the metal-centered p-π orbital

Table 3. Calculated (B3LYP) and Observed Frequencies (cm^{-1}), Symmetries, and Intensities (km/mol) for Known Group I and II Metal−Methyl Species

isotopomer	calcd frequencies (cm^{-1}), symmetries, and intensities (km/mol)			obsd frequencies (cm^{-1})		
$^{7}LiCH_3$[a]	449.4, e (173) × 2;	627.5, a_1 (26);	1137.3, a_1 (1);	408.5,	530,	1158,
	1477.9, e (1) × 2;	2950.4, a_1 (97);	3005.2, e (53) × 2	1387,	2780,	2820
$^{7}Li^{13}CH_3$	447.0, e;	620.9, a_1;	1130.2, a_1;		not observed	
	1474.7, e;	2947.3, a_1;	2995.1, e			
$^{7}LiCD_3$	345.6, e;	608.8, a_1;	872.0, a_1;	319,	510,	883
	1071.6, e;	2116.2, a_1;	2218.4, e	1027,	2030	
$^{6}LiCH_3$	451.7, e;	662.1, a_1;	1137.3, a_1;	410.7,	558,	1158,
	1477.9, e;	2950.4, a_1;	3005.2, e	1387,	2780,	2820
$^{6}Li^{13}CH_3$	450.7, e;	654.1, a_1;	1130.5, a_1;	~550 (a_1)		1152 (a_1)
	1474.8, e;	2946.4, a_1;	2994.1, e			
$^{6}Li\ CD_3$	348.6, e;	643.9, a_1;	872.5, a_1;	323,	536,	886,
	1071.6, e;	2116.2, a_1;	2218.4, e	1027,	2030	
$BeCH_3$[b]	580.6, e (1) × 2;	72.1, a_1 (27);	1251.5, a_1 (41);	851.7 (a_1),		1180 (a_1)
	1460.8, e (10) × 2;	2990.2, a_1 (7);	3053.5, e (10) × 2			
$Be^{13}CH_3$	577.4, e;	862.7, a_1;	1240.8, a_1;	843.8,		1170
	1458.1, e;	2986.5, a_1;	3042.8, e			
$BeCD_3$	450.3, e;	791.5, a_1;	1018.0, a_1;	765.6,		962.1
	1056.1, e;	2148.4, a_1;	2255.1, e			
$NaCH_3$[c]	386.5, a_1 (11);	454.9, e (121) × 2;	1027,3, a_1 (127);	298,	362,	1092,
	1470.3, e (1) × 2;	2988.3, a_1 (144);	3069.9, e (35) × 2	1384,	2760,	2805
$NaCD_3$	339.1, e;	366.4, a_1;	787.9, a_1;	278,	285,	836,
	1069.1, e;	2136.7, a_1;	2271.4, e	972,	2019,	2123
$^{24}MgCH_3$[d]	473.4, a_1 (13);	520.4, e (1) × 2;	117.7, a_1 (11);	509 (e),		1072(a_1)
	1465.7, e (6) × 2;	2998.5, a_1 (60);	3080.0, e (20) × 2			
$^{26}MgCH_3$	466.3, a_1;	520.1, e;	1117.7, a_1;		not observed	
	1465.7, e;	2998.5, a_1;	3080.0, e			
$^{24}Mg^{13}CH_3$	463.8, a_1;	517.9, e;	1110.8, a_1;		not observed	
	1462.5, e;	2995.8, a_1;	3069.0, e			
$^{24}MgCD_3$	448.5, a_1;	390.1, e;	855.9, e;		not observed	
	1063.5, a_1;	2146.6, a_1;	2278.6, e			
KCH_3[c]	293.8, a_1 (23);	346.0, e (110) × 2;	1026.4, a_1 (180);	280,	307,	1053,
	1471.1, e (1) × 2;	2956.3, a_1 (251);	3028.2, e (61) × 2	1384,	2732,	2775
KCD_3	256.9, e;	276.8, a_1;	782.8, a_1;	237,	259,	807,
	1069.7, e;	2115.3, a_1;	2238.4, e	967,	1994,	2101
$CaCH_3$[e]	382.3, e (1) × 2;	414.5, a_1 (25);	1155.6, a_1 (6);	419 (a_1),		1085
	1466.3, e (8) × 2;	2947.1, a_1 (96);	3007.6, e (25) × 2			
$CaCD_3$	284.1, e;	386.6, a_1;	886.7, a_1;		not observed	
	1063.6, e;	2116.1, a_1;	2222.5, e			

[a] Observed in solid argon, ref 21. [b] Observed in solid argon, ref 1. [c] Observed in solid nitrogen, ref 23. [d] Observed in gas phase, ref 22. [e] Observed in gas phase, ref 25.

for the $XMCH_2$ species; however, there is no significant increase in metal−carbon π bonding relative to MCH_2 and $HMCH_2$. The metal−carbon bond strengths are also comparable to those of the $HMCH_2$ molecules. This similarity in bond energy indicates that any perturbations to the overall bonding interaction resulting from additional electrons donated to the b_1 and b_2 orbitals by the halogen atoms are negligible relative to the increased σ bond strength which results from sp hybridization of the metal atom.

Summary of Bonding

Figure 3a summarizes the metal-to-methylene charge transfer in all $X-M-CH_2$ species. The MCH_2 species display essentially complete donation of a β electron from the metal to CH_2, with minor back-donation of an α electron to the metal. For all other $XMCH_2$ species, there is a partial transfer to the methylene of roughly equivalent amounts of α and β charge.

The participation of metal-centered p orbitals for the MCH_2, $HMCH_2$, and $XMCH_2$ species is summarized in Figure 3b, which displays the electron occupation of each orbital in both α and β manifolds, as determined by DFT/NBO calculations. Although the p occupation is very small in all cases, there are discernible trends and deviations which warrant discussion. First, we note that the p-pseudo π (b_2) orbitals have nearly equal participation in the α and β manifolds for all species discussed here. This participation is zero for both α and β manifolds for MCH_2 species and gradually increases for $HMCH_2$ and $XMCH_2$. In stark contrast to this is the marked difference in the occupation of p-σ (a_1) orbitals in the α and β manifolds of $BeCH_2$ and $MgCH_2$. In these molecules the p-σ participation is relatively large in the α manifold and zero in the β manifold. For all other species, the α/β occupation is nearly identical, with a slightly greater p-σ occupation in the β manifold.

The most significant trend is in the α and β occupation of the p-π (b_1) orbitals, which are clearly inequivalent for all species discussed here. For the MCH_2 and $HMCH_2$ species, calculations indicate a much greater electron occupation in the α manifolds, which results from electron donation from the carbon p-π orbital to the metal. For the $XMCH_2$ radicals, there is nonnegligible participation in both manifolds; however, in all cases this participation is slightly (for Mg species) or substantially (for Be species) greater in the α set. For the $XMCH_2$ species, the metal-centered p-π participation in the β manifold results only from interactions with the halogen atom (as C has no b_1 electron in the β manifold), whereas in the α manifold contributions from both the halogen and carbon atoms are important. For this reason, the *difference* between the p-π participation in the α and β manifolds gives a measure of the extent of p-π bonding with carbon.

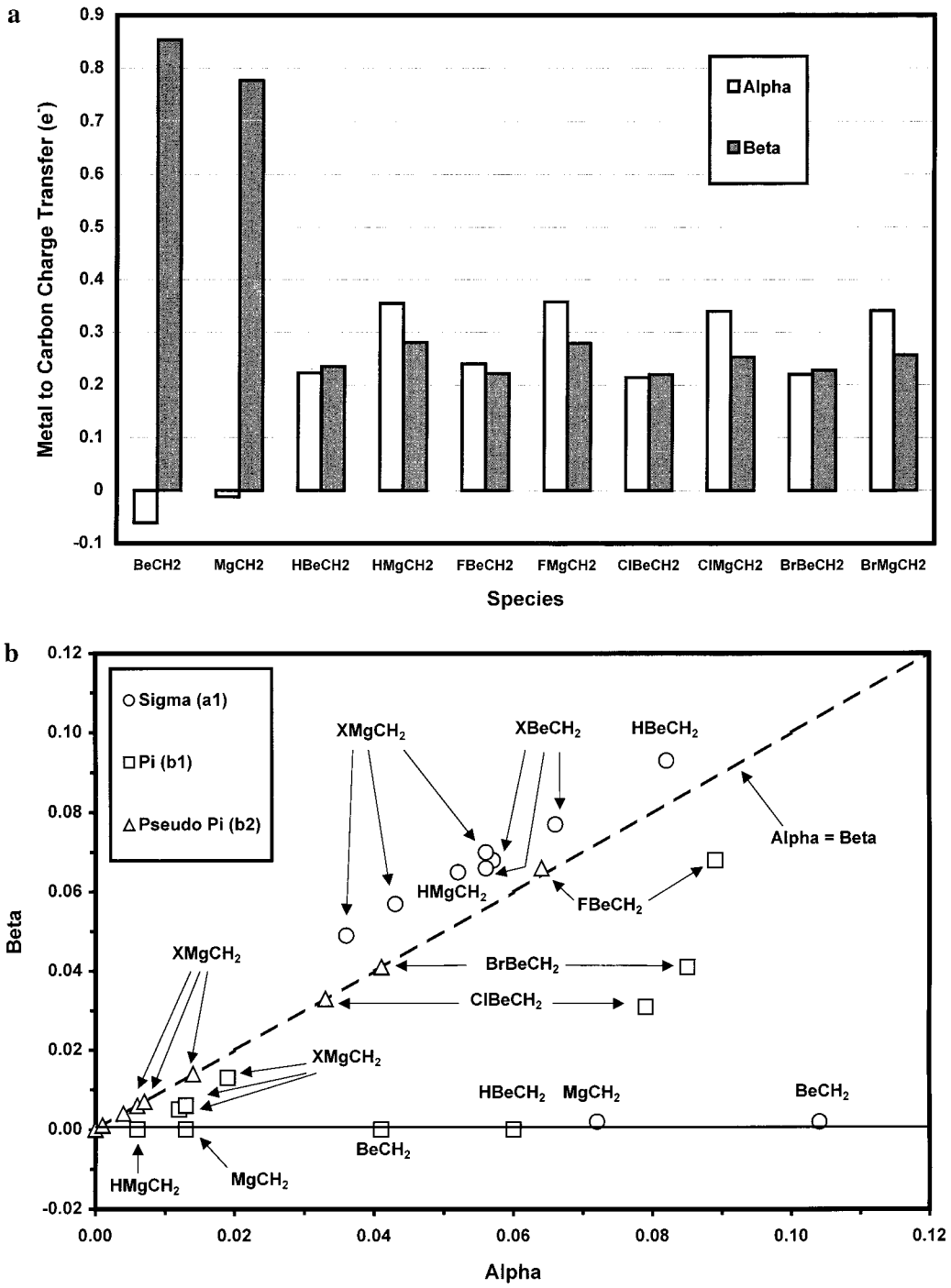

Figure 3. (a) NBO-calculated charge transfer from metal (or X−metal fragment) to methylene for all MCH_2, $HMCH_2$, and $XMCH_2$ species in both α and β electron manifolds. (b) NBO-calculated electron occupation of metal-centered p orbitals for beryllium and magnesium carbene and carbenoid species.

Measured Infrared Spectra and Assignments

Reaction products from laser-ablated magnesium atoms with methane and methyl halides were isolated in argon matrixes and analyzed by infrared spectroscopy. Spectra from the magnesium experiments with methane and methyl halides of particular interest are presented in Figures 4−6. Infrared absorptions of products are collected in Table 4. Infrared absorptions are assigned on the basis of isotopic shifts and correlation with DFT calculations.

$XMgCH_2$. Molecules with the $XMgCH_2$ structure were formed in experiments with all three methyl halides discussed here. Spectra showing IR absorptions due to these $XMgCH_2$ species are shown in Figure 4. In all cases, the C−Mg−X antisymmetric stretch is predicted to be the most intense vibrational mode and was the only IR absorption observed for these species. These bands were approximately 20−50 cm^{-1} higher than the similar stretching mode of the analogous Grignard species.[2] Although only one band was observed for each of these species, the excellent agreement between observed and calculated frequencies (scale factor 0.99) and isotopic ratios (as shown in Table 5) confirms their assignments.

The antisymmetric F−Mg−C stretches of four isotopomers of the fluorine carbenoid, $FMgCH_2$, were identified. Reactions with methyl chloride produced three bands (663.0, 655.7, and

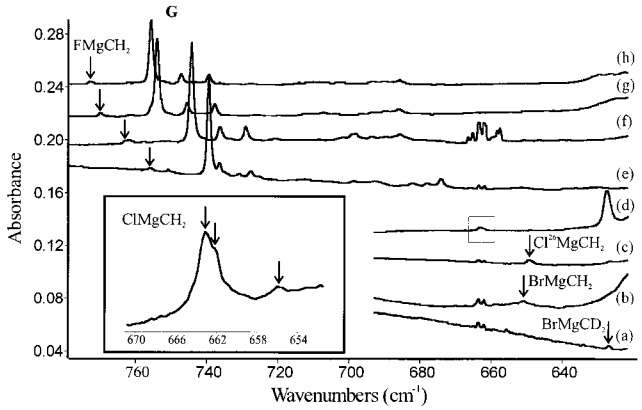

Figure 4. Infrared spectra in the 800−620 cm^{-1} region for laser-ablated Mg atoms codeposited with CH_3X molecules in excess argon onto a 10 K CsI window. Spectra shown here were recorded following annealing to 25 K. Peaks labeled "G" are due to Grignard species and have been discussed in ref 2. (a) CD_3Br + Mg. (b) CH_3Br + Mg. (c) CH_3Cl + ^{26}Mg. (d) CH_3Cl + Mg. (e) CH_3F + ^{26}Mg. (f) CD_3F + Mg. (g) $^{13}CH_3F$ + Mg. (h) CH_3F + Mg.

649.3 cm^{-1}) with an 8:1:1 intensity ratio, which is indicative of isotopic splitting arising from Mg isotopes (24, 25, 26) in natural abundance. These bands were identified as $Cl^{24}MgCH_2$, $Cl^{25}MgCH_2$, and $Cl^{26}MgCH_2$, respectively. The strongest band exhibited a partially resolved shoulder at 662.1 cm^{-1}, which is assigned to $^{37}Cl^{24}MgCH$. Two isotopomers, $BrMgCH_2$ and $BrMgCD_2$, of the bromine species were observed at 650.9 and 626.4 cm^{-1} . The broadness of the bands due to $BrMgCH_2$ and $BrMgCD_2$ is not unexpected. Our previous investigation on Grignard species[2] indicates that this is a general trend, namely, that the broadness of X−Mg−CH_n stretches increases in the order F < Cl < Br < I. This may be due to the larger variability in matrix sites required by larger molecules, or it may reflect the increasing polarizability of bromine- and iodine-containing species, which makes them more susceptible to perturbation by nearby guest molecules. For all of these molecules, the observed frequencies show excellent agreement with calculated frequencies. More importantly, however, the many observed frequency *shifts* resulting from isotopic substitution convey much more molecule-specific information than the frequencies themselves and are in superb agreement with those calculated for these C_{2v} species. We note that the only disagreement is a very slight anomaly in the calculated deuterium shift, which may indicate a slight miscalculation of the extent of charge delocalization from XMg to CH_2, as will be discussed below.

$MgCH_2$. In experiments employing laser-ablated magnesium atoms and methyl halides, a halogen-independent band was observed at 502.2 cm^{-1} and showed isotopic shifts resulting from substitution with ^{26}Mg, ^{13}C, and D which are appropriate for a Mg−C stretching mode. This band tracked with a band at 2787.1 cm^{-1} and always exhibited an integrated intensity approximately 3 times that of the upper band. Spectra showing the 502.2 and 2787.1 cm^{-1} bands in experiments with both methane and methyl halides are shown in Figure 5. These spectra show important isotopic (^{26}Mg, ^{13}C, and D) shifts and make clear the lack of halogen dependence, with both upper and lower bands appearing unshifted for experiments with methane and three different methyl halides.

The 502.2 cm^{-1} band was also observed by Greene and coworkers in experiments with laser-ablated magnesium and methane.[1] The methane experiments were repeated here under conditions necessary to maximize the yield of the 502.2 cm^{-1} band and sample transmission in the 2800 cm^{-1} region. These experiments were done under conditions of lower laser power with fewer metal atoms present, which makes the formation of a dimagnesium species unlikely. In these experiments, the 2787.1 cm^{-1} band was observed with the same intensity ratio as seen in the methyl halide experiments. The tracking behavior of these two bands is seen in Figure 6, which shows both bands being unaffected by photolysis and by low-temperature (25−30 K) annealing. Both bands decrease by approximately 50% following high-temperature (35 K) annealing. Note that the nearby $HMgCH_3$ bands undergo much greater fluctuation.

These results indicate that the 502.2 and 2787.1 cm^{-1} bands are due to absorptions of either an $HMgCH_n$ or $MgCH_n$ species. The former molecules can be ruled out because no Mg−H stretching mode was found that tracked with these bands. $HMgCH_3$ has, in fact, been observed previously in a solid methane matrix[18] at approximately 539 cm^{-1} accompanied by a strong Mg−H stretch at 1524 cm^{-1}. In solid argon, this molecule shows a Mg−C stretch near 545 cm^{-1} and an intense Mg−H stretch at 1560.3 cm^{-1}. For $HMgCH_2$, the Mg−H stretch is expected to be more intense than the Mg−C stretching mode by a factor of 6 and should be observed if a molecule with this structure were formed.

Of the two likely $MgCH_n$ species, the observed frequency and isotopic shifts for the 502.2 cm^{-1} band are more consistent with the calculations for $MgCH_2$ (Table 1) than with similar calculations for $MgCH_3$ (Table 5), which predict a Mg−C stretching mode at 473.4 cm^{-1} and an equally strong methyl deformation mode at 1117.7 cm^{-1} that are not found here. Recent observation[19] of $MgCH_3$ fundamentals ν_2 (a_1 symmetric umbrella) at 1072 cm^{-1} and ν_6 (e, antisymmetric H−C−Mg wag) at 509 cm^{-1} support the predictive ability of the DFT calculations in Table 3. No such band is observed in these experiments. We also note that the spectral region from 1000 to 1200 cm^{-1} is very clean in the methane experiments performed here, and no methyl deformation mode was found corresponding to the previously observed 1117.7 cm^{-1} band. We conclude that the 502.2 and 2787.1 cm^{-1} bands are due to the Mg−C and C−H stretches of $MgCH_2$.

Performance of DFT Models for Mg Species

All calculated frequencies are unscaled roots of the second derivative matrix of the potential energy, referring to mass-weighted displacement coordinates. They are approximations to harmonic frequencies, while observed transition frequencies of course incorporate some anharmonicity. As mentioned above, the DFT modeling of stretching frequencies of $XMgCH_2$ species is remarkably faithful. The calculated and *unscaled* frequencies are essentially identical (within 10 cm^{-1}) with observed values, the isotopic shifts are well reproduced, and even the intensities are of semiquantitative value. Linear regression of calculated vs observed frequencies for $XMgCH_2$ yields a statistic R^2 (the square of the correlation coefficient) of 0.9987 and a standard error in the computed frequencies of 2 cm^{-1}.

The performance of DFT methods for $MgCH_2$ is less consistent, and several disparities must be addressed. The observed ^{13}C shift (5.8 cm^{-1}) for the C−H stretching mode at 2787.1 cm^{-1} is in excellent agreement with the calculated value (5.5 cm^{-1}); however, the observed frequency of the C−H stretching mode at 2787.1 cm^{-1} is lower by almost 250 cm^{-1}

(18) McCaffrey, J. G.; Parnis, J. M.; Ozin, G. A.; Breckinridge, W. H. *J. Phys. Chem.* **1985**, *89*, 4945.
(19) Rubino, R.; Williamson, J. M.; Miller, T. A. *J. Chem. Phys.* **1995**, *103*, 5964. Salzberg, A. P.; Applegate, B. E.; Miller, T. A. *J. Mol. Spectrosc.* **1999,** *193*, 434.

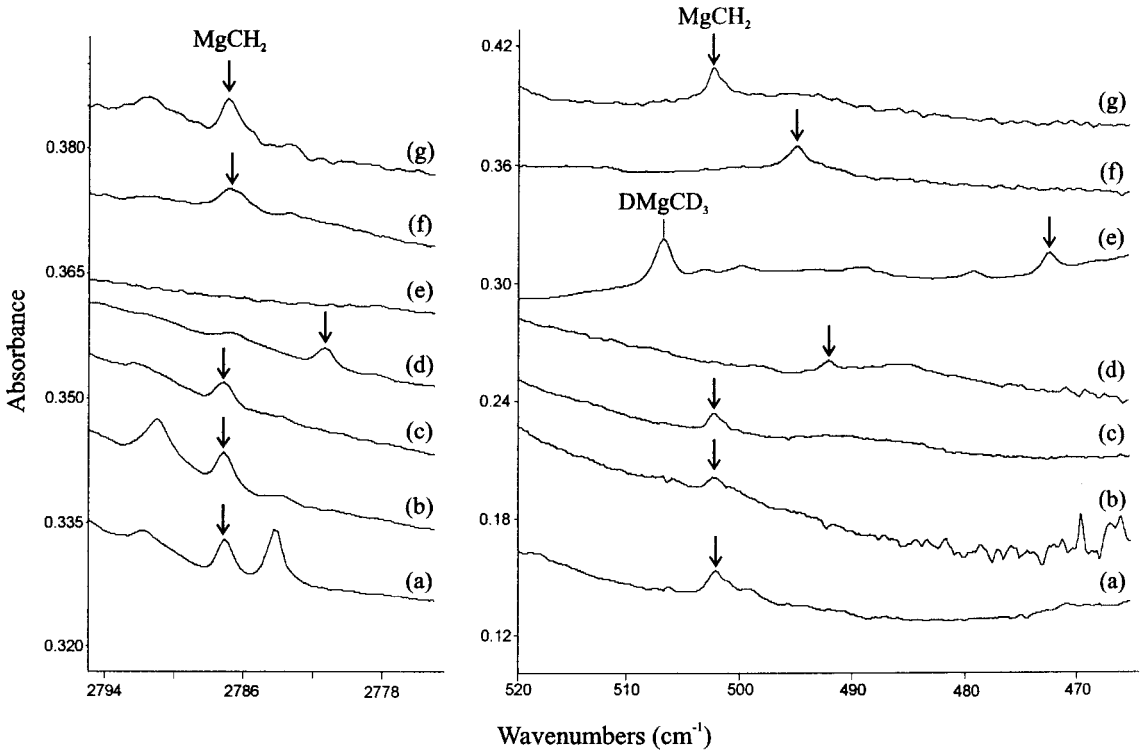

Figure 5. Infrared spectra in the 2795−2775 and 520−460 cm^{-1} regions for laser-ablated Mg atoms codeposited with CH_3X or CH_4, diluted in argon and condensed on a 10 K CsI window. Spectra shown here were recorded following annealing to 25 K. (a) CH_3Br + Mg. (b) CH_3Cl + Mg. (c) CH_3F + Mg. (d) $^{13}CH_3F$ + Mg. (e) CD_4 + Mg. (f) CH_4 + ^{26}Mg. (g) CH_4 + Mg.

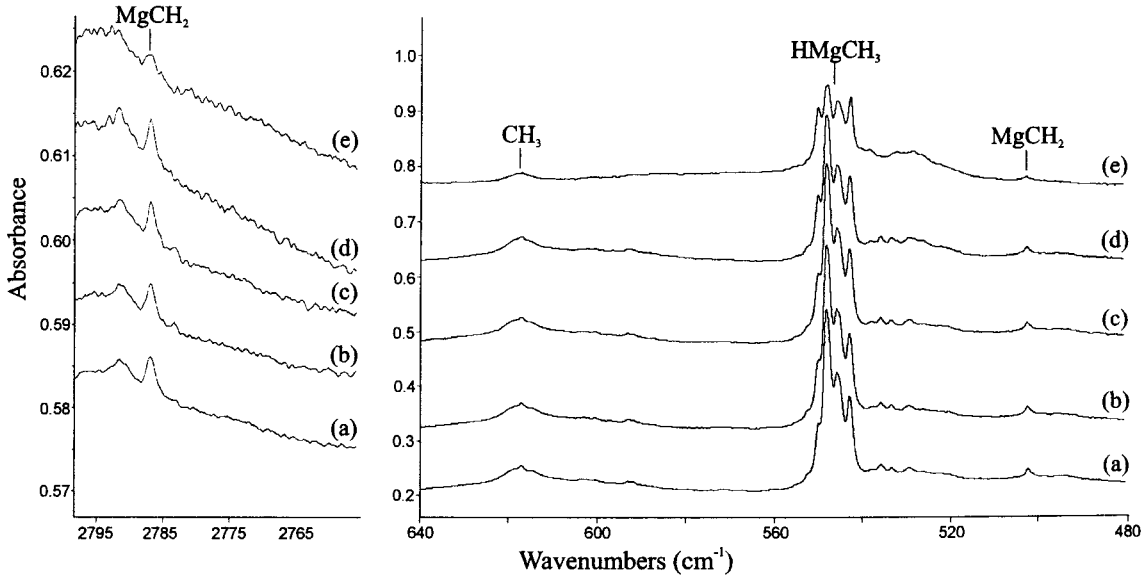

Figure 6. Infrared spectra in the 2797−2760 and 640−480 cm^{-1} regions for laser-ablated Mg atoms codeposited with CH_4 diluted in excess argon on a 10 K CsI window. Spectra are recorded following (a) deposition, (b) annealing to 25 K, (c) broadband photolysis, (d) annealing to 30 K, and (e) annealing to 35 K.

than the frequency predicted by DFT/6-311+G* calculations (3032.6 cm^{-1}). The ratio of observed/calculated frequencies of 0.92 is significantly lower than the 0.96 scale factor typical of B3LYP calculations of C−H stretching modes.[20] This band is also some 150 cm^{-1} lower than the C−H stretching bands observed previously[3,4] for transition metal carbene complexes. Although the observed C-13 and Mg-26 shifts (10.1 and 7.3 cm^{-1}, respectively) for the 502.2 cm^{-1} band are in excellent agreement with the calculated values for $MgCH_2$, the observed deuterium shift (29.8 cm^{-1}) is significantly larger than that predicted (23.2 cm^{-1}) by the DFT calculations. Finally, assignment to the $MgCH_2$ molecule is also complicated by the failure to observe an out-of-plane bending mode which is predicted at about 610 cm^{-1}. Each of these inconsistencies can be explained as stemming from a specific error in the calculations, and this explanation is supported by comparison to similar known molecules.

Special Considerations for Calculations of Highly Ionic Species

Some discrepancies between observed and calculated frequencies and intensities are to be expected, particularly for

(20) Choi, C. H.; Kertesz, M. *J. Phys. Chem.* **1996**, *100*, 16530.

Table 4. Infrared Bands (cm^{-1}) Observed for Magnesium Carbene and Carbenoid Radicals in Solid Argon

$^{n}Mg + CH_3X$	$^{26}Mg + CH_3X$	$^{n}Mg + CD_3X$	$^{n}Mg + {}^{13}CH_3X$	assignment
502.2	494.9	472.1	492.1	$MgCH_2$ (a_1)
555.3		429.0		$BrMgCH_3$ (e)
556.6	556.3			$ClMgCH_3$ (e)
561.3	560.8			
557.8	557.2	428.9	554.7	$FMgCH_3$ (e)
560.2	559.6	431.3	557.0	
627.1	612.9			$ClMgCH_3$ (a_1)
650.9		626.4		$BrMgCH_2$ (a_1)
663.0				$^{35}Cl^{24}MgCH_2$ (a_1)
662.1				$^{37}Cl^{24}MgCH_2$ (a_1)
655.7				$^{35}Cl^{25}MgCH_2$ (a_1)
649.3	649.3			$^{35}Cl^{26}MgCH_2$ (a_1)
755.8	739.6	744.5	754.1	$FMgCH_3$ (a_1)
772.9	756.1	762.9	770.2	$FMgCH_2$ (a_1)
2787.1	2786.8	2040.3	2781.3	$MgCH_2$ (a_1)

Table 5. Calculated (B3LYP/6-311+G*) and Observed (in Solid Argon at 10 K) Isotopic Frequencies and Frequency Ratios for the Antisymmetric C−Mg−X Stretch of $XMgCH_2$ Radicals

isotopomer	calcd frequency	obsd frequency	calcd frequency ratio	obsd frequency ratio
$F^{24}MgCH_2$	777.3	772.9		
$F^{24}Mg^{13}CH_2$	774.2	770.2	1.004	1.004
$F^{24}MgCD_2$	768.6	762.9	1.011	1.013
$F^{26}MgCH_2$	759.9	756.1	1.023	1.022
$^{35}Cl^{24}MgCH_2$	668.6	663.0		
$^{37}Cl^{24}MgCH_2$	667.8	662.1	1.001	1.001
$^{35}Cl^{25}MgCH_2$	661.2	655.7	1.011	1.011
$^{35}Cl^{26}MgCH_2$	654.2	649.3	1.022	1.021
$Br^{24}MgCH_2$	650.0	650.9		
$Br^{24}MgCD_2$	626.9	626.4	1.037	1.039

species with highly ionic bonds. To provide a context for judgment of the reliability of DFT frequency calculations for highly polar molecules, we assembled results for $LiCH_3$,[21,22] $NaCH_3$,[23] KCH_3,[23,24] $MgCH_3$,[19] and $CaCH_3$,[25] all of which are experimentally known.

A moderate overestimate of the C−H stretching frequency is to be expected for organic or organometallic species, and familiar scaling rules of thumb are the usual way to recognize and allow for this systematic error. However, our observation that the C−H stretch in $MgCH_2$ is anomalously overestimated by DFT/6-311+G* suggests that the effects on the C−H bond of the very polarized metal to carbon bonds are very difficult to model quantitatively and warrants special attention. We first note that C−H bonds involve net electron donation from H to C, and so it is not unreasonable to expect some weakening of the C−H bond to result from an accumulation of negative charge on the carbon atom. In fact, Figure 7 shows that weakening of the C−H bond as charge is donated to carbon is recognized in part in DFT calculations. For example, B3LYP/6-311+G* computes the antisymmetric C−H stretch in methyl anion as 2951 cm^{-1}, as opposed to 3121 cm^{-1} for the antisymmetric stretch in methyl fluoride and 3096 for the motion in ethane.

In general, for MCH_3 species, we observe a correlation in the data between charge on a methyl group and the frequency

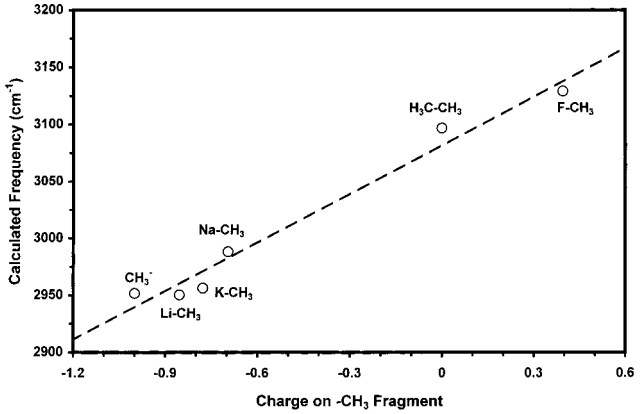

Figure 7. Calculated (B3LYP/6-311+G*) antisymmetric C−H stretching frequencies (cm^{-1}) as a function of charge (NBO) on the organic fragment.

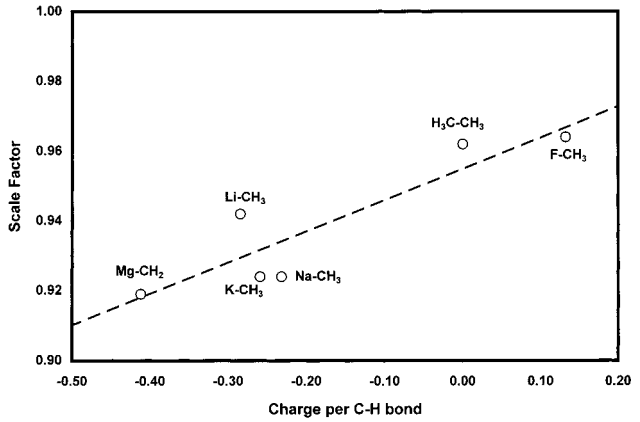

Figure 8. Calculational scaling factors (observed frequency/calculated frequency) displayed as a function of charge distributed per C−H bond.

of its asymmetric C−H stretch for both calculated and observed frequencies. Negative charge red-shifts the frequency of the mode, and positive charge induces a blue-shift. Further, although the calculations do recognize this red-shift, the accuracy of the calculation becomes increasingly poor as charge accumulates. We reason that the effect of the charge accumulation is distributed evenly among the C−H bonds, and that the miscalculation of bond stretching frequencies is magnified either by increased charge or by distributing this effect over fewer bonds. Figure 8 shows that as the charge on the organic fragment accumulates, the scaling factors that are required to bring calculated frequencies into agreement with experimental results deviate farther from unity. Regression analysis of the observed/calculated scale factors as a function of charge per C−H bond gives an R^2 value of 0.812, which is reasonable for this small data set. It appears that the B3LYP/6-311+G* method cannot accurately represent the large charge delocalization from the metal atom to carbon in these molecules. As a result, the negative charge on the carbon atom is underestimated, and the C−H bond strength is overestimated. Finally, we note that B3LYP/6-311++G** calculations on methylene doublet anion produce a lengthened C−H bond (1.126 Å) and an unscaled frequency of 2702 cm^{-1}.

It appears that our conclusion on the bonding in the $MgCH_2$ system, that it is very nearly approximated as to two triplet-coupled radicals (Mg^+ cation and CH_2^- π-doublet anion), is fully consistent with experimental data. The calculations on the CH stretches of $MgCH_2$ are, however, not satisfactory.

The faulty description of the charge distribution in very polar bonds has a significant but confusing effect on the frequency

(21) Andrews, L. *J. Chem. Phys.* **1967**, *47*, 4834.
(22) Grotjahn, D. B.; Pesch, T. C.; Xin, J.; Ziurys, L. M. *J. Am. Chem. Soc.* **1997**, *119*, 12368.
(23) Burczk, K.; Downs, A. J. *J. Chem. Soc., Dalton Trans.* **1990**, 2351.
(24) The 6-311+G* basis set used for K was that given by Bladeau et al. Bladeau, J.; McGrath, P.; Curtiss, L. A.; Radom, L. *J. Chem. Phys.* **1997**, *107*, 5016.
(25) Brazier, C. R.; Bernath, P. F. *J. Chem. Phys.* **1987**, *86*, 5918. Brazier, C. R.; Bernath, P. F. *J. Chem. Phys.* **1989**, *91*, 4548.

Table 6. Density Functional (B3LYP) Calculations for the $MgCH_2$ Molecule in "Balanced" Basis Sets[a]

basis on CH_2 (Mg has 6-31G)	6-31G*	6-31+G**	6-311++G**	exptl
energy (hartrees)	−239.28496	−239.29245	−239.30068	
Mg−CH_2 bond energy (kcal/mol)	36	35	35	
Mulliken charge	0.368	0.492	0.491	
NBO charge	0.687	0.748	0.758	
freq C−H stretch[a]	3073	3063	3042	2787
freq C−D stretch[a]	2227	2218	2203	2040
freq Mg−CH_2 stretch[a]	539	530	524	502
freq Mg−CD_2 stretch[a]	516	508	502	472
D-shift (Mg−CH_2 stretch)	−23	−22	−22	−30
intensity of Mg−CH_2 stretch	21.5	32.9	35.7	
rel intensity Me wag/ Mg−CH_2 stretch	4.2	2.9	2.5	not seen

[a] Reported frequencies are not scaled.

of the M−CH_n stretching mode. The frequency of the mode is drastically (ca. 20%) overestimated for $LiCH_3$, $NaCH_3$, and $HMgCH_3$, while a fairly good agreement is observed for the $CaCH_3$ and $BeCH_3$ radicals and for singlet KCH_3. The isotopic shifts are also fairly well described, although D-shifts are *systematically underestimated*. For all known group I and II MCH_3 species, the ratio of the calculated H/D ratio to the observed H/D ratio falls in the range 0.981−0.990. The ratio for $MgCH_2$ is 0.983.

The relationship between the C−H stretching frequency and the deuterium shift of the M−C mode is easily seen by comparison to a hypothetical Mg−CH_2 molecule with infinitely stiff C−H bonds. For this molecule, the deuterium shift of the M−C stretch may be calculated by assuming a diatomic molecule with atomic weights of 24 − 14 and 24 − 16 for the natural and deuterium-substituted species, respectively. In this hypothetical case, a deuterium shift of only 20 cm^{-1} is expected, which is well below both the calculated and observed values. Therefore, both the calculations and experimental results indicate a significant coupling of the Mg−C and C−H vibrations in this molecule. When the importance of coupling between these two modes is understood, we are no longer surprised that the D-shift of the Mg−methylene stretch and the fundamental frequency of the C−H stretches are *both* underestimated in the DFT representation. The weakness of the C−H bond, underappreciated in the modeling, has the effect of enhancing deuterium shifts of other modes by stronger coupling than the modeling can capture. The same failing explains another deficit of the modeling.

According to the calculations done here, the $MgCH_2$ molecule should have an out-of-plane bending motion near 610 cm^{-1}, which is estimated (B3LYP/6311+G*) to be approximately 2× as intense an absorber as the Mg−C stretch. No such band has been observed. This spectral region is complicated by several absorptions, and the bending mode may be obscured by the very strong bend of $HMgCH_3$ and $XMgCH_3$ molecules or by the methyl radical.[26] There is also good reason to believe that this bending mode may be much less intense than indicated by DFT calculations. If the polarity of the M−C bond is poorly characterized by the B3LYP/6-311+G* calculation and the extent of charge delocalization is actually larger than calculated, then the dipole moment of the molecule will also be larger than calculated, as will be the oscillator strength of the Mg−C vibration. One may then conjecture that the Mg−C stretch may even be stronger than the out-of-plane bend. If so, it is not unreasonable that an absorption band for the bending mode is not observed here. This argument is supported by the observed intensities of the modes of $LiCH_3$.

For $LiCH_3$, the observed intensities of the C−H stretch and methyl wag are approximately $^1/_6$ and $^1/_{20}$ of the predicted intensities relative to the Li−C stretch. In $MgCH_2$, the observed C−H stretching mode is approximately $^1/_3$ the intensity of the Mg−C stretch, instead of twice as intense, as predicted, indicating a substantial underestimation of the Mg−C oscillator strength. On the basis of this data, it is not at all unreasonable to suggest that the actual intensity of the methylene wag is much lower than that of the Mg−C stretch and may well be too small to be observed, particularly in such a crowded spectral region.

Balancing the Metal and Carbon Basis Sets

All the calculations described so far use a standard basis. To take an example which is not too cumbrous, we consider the standard 6-31G* basis set. Any calculation using a 6-31G* basis splits the valence set and adds a high-angular-momentum set of polarization functions. For carbon, a d orbital serves as the polarization function. In some (**) basis sets a p function is placed on hydrogen atoms, also for polarization.

In a metal−carbene or carbenoid system, any standard basis is severely biased in favor of the metal. To see this, consider the carbon. A minimum representation of C's valence electrons requires occupation of the 2s and 2p orbital manifold. The 6-31G* basis adds d orbitals to allow polarization of the s,p set. However a minimum representation of the valence electrons of magnesium requires only the 3s orbital. The 3p manifold would provide effective polarization of the s-electrons; however, the 6-31G* basis further adds a set of d functions. Therefore, the *effective flexibility* of the 6-31G* basis for Mg is greater than for carbon in the same basis. In the variation calculation the Mg basis is employed to describe the neighborhood of the carbon atom, so as to find the molecule's lowest energy, and this inevitably works against a proper description of the distribution of charge between such different adjacent sites.

One might hope to achieve a better description by attempting to "balance" the basis set, allowing a nonpolarized set of functions on the Mg virtual cation and a more flexible basis on the methylene virtual anion. To explore this possibility, we conducted a series of calculations with a 6-31G basis on Mg and more flexible sets on the C and H atoms. As Tables 6 and 7 show, charge transfer toward the "anion" is more complete as the basis set at that site becomes more flexible and hospitable, and the prediction of frequencies improves as the "anionic" site is better described. The Mg−methylene stretching frequency also decreases, approaching the observed value to within 3−4% for the largest anion basis 6-311++G**.

Our conjecture that there would be an impact of the weakened C−H bond on the relative intensities of the b_1 pyramidalization band predicted at about 610 cm^{-1} and the a_1 Mg−C stretching

(26) Milligan, D. E.; Jacox, M. E. *J. Chem. Phys.* **1967**, *47*, 5146.

Table 7. Complete Active Space Calculation for the $MgCH_2$ Molecule in "Balanced" Basis Sets Using CASSCF (8,8)

basis on CH_2 (Mg has 6-31G*)	6-31G*	6-31+G**	6-311++G**	exptl
energy (hartrees)	−238.60588	−238.61215	−238.61963	
Mg−CH_2 bond energy (kcal/mol)	15	15		
Mulliken charge	0.448	0.613	0.600	
NBO charge	0.748	0.794	0.804	
freq C−H stretch	2996	2983	2954	2787
freq C−D stretch	2178	2169	2140	2040
D-shift (C−H stretch)	−813	−814	−814	−747
freq Mg−CH_2 stretch	532	525	519	502
freq Mg−CD_2 stretch	508	503	491	472
D-shift (Mg−CH_2 stretch)	−22	−22	−22	−30
intensity Mg−CH_2 stretch	30.3	37.8	42.0	
rel intensity Me wag/Mg−CH_2 stretch	2.52	2.13	1.77	not seen

Table 8. Effect of "Balanced" Basis Set Calculations for the $LiCH_3$ Molecule Using DFT (B3LYP)

	6-31G*	6-31+G**	6-311++G**	exptl
energy (hartrees)	−47.39986	−47.40853	−47.41688	
Mulliken charge	0.387	0.386	0.298	
NBO charge	0.756	0.831	0.835	
freq of e modes (cm^{-1})	501 (388)	481 (372)	466 (360)	449
(parenthetical values are for	1493 (1082)	1457 (1057)	1453 (1055)	1478
for deuterated species)	3051 (2253)	3046 (2250)	3028 (2236)	3005
freq of a_1 (cm^{-1})	661 (644)	643 (627)	630 (614)	628
(parenthetical values are	1143 (877)	1103 (847)	1094 (841)	1137
for deuterated species)	2985 (2139)	2976 (2133)	2966 (2125)	2950
D-shift (Li−CH_3 stretch)	−17	−16	−16	−22
intensity of Li−CH_3 stretch	12.4	26.3	28.9	
rel intensity Me wag/Li−CH_3 stretch	18.8	6.7	5.8	∼2

Table 9. Effect of "Balanced" Basis Set Calculations for the $LiCH_3$ Molecule Using CASSCF (8,8)

basis on CH_3 (Li has 6-31G)	6-31G*	6-31+G**	6-311++G**	exptl
energy (hartrees)	−47.1031	−47.1104	−47.1179	
Mulliken charge	0.406	0.396	0.309	
NBO charge	0.743	0.804	0.808	
freq of e modes (cm^{-1})	510 (392)	482 (368)	465 (357)	449
(parenthetical values are	1526 (1110)	1495 (1088)	1486 (1081)	1478
for deuterated species)	2985 (2213)	2983 (2211)	2956 (2190)	3005
freq of a_1 modes (cm^{-1})	601 (585)	583 (568)	576 (568)	628
(parenthetical values are	1187 (911)	1138 (873)	1127 (866)	1137
for deuterated species)	2915 (2096)	2905 (2087)	2882 (2071)	2950
D-shift for Li−CH_3 stretch	−16	−15	−8	−22

band at 520−540 cm^{-1} is supported by these DFT balanced basis calculations. The intensity ratio (600 cm^{-1} band/500 cm^{-1} band) decreases from 4.2 to 1.7 as the basis on methylene is expanded from 6-31G* to 6-311++G**.

Basis set flexibility alone is not the entire remedy, however. A serious treatment of correlation is needed to deal with the weakening of the CH bond in the effective anion. DFT does incorporate a treatment of correlation energy, but does not fully capture the weakening of the CH bond. Our balancing trick improved matters only modestly. CASSCF(8,8) calculations correlate all the electrons in the valence shell. (The method does not, however, include "dynamic correlation" as MP2 does by including admixture of states outside the valence manifold, or as DFT seems to be able to manage.) The CAS calculations, shown in Table 7, were fairly successful in predicting the C−H weakening, reducing the error to about 100 cm^{-1}, while the best DFT result was in error by almost 250 cm^{-1}. Consequently the observed 747 cm^{-1} isotopic shift in the CH/CD symmetric stretches was better predicted in CAS (814 cm^{-1}) than DFT (849 cm^{-1}). The DFT- and CAS-calculated shifts for the Mg−methylene stretch were in perfect agreement, but at 22 cm^{-1} still seriously short of the observed 30 cm^{-1}.

Parallel calculations on methyllithium (Tables 8 and 9) gave generally analogous results, but the more complete data available for methyllithium allows more sweeping statements. Generally DFT provides a better match to spectra than CAS in small basis sets for the methyl anion fragment. At the 6-311++G** level, the two computational descriptions are entirely consistent, with a statistic R^2 of 0.99 or better in all cases and with the best standard error in unscaled predicted frequency being about 30 cm^{-1} in each case.

Conclusions

The reaction of laser-ablated magnesium atoms with methyl halides produced carbenoid radicals ($XMgCH_2$) and the magnesium carbene ($MgCH_2$), in addition to other products reported earlier. These carbene and carbenoid species have been identified and their vibrational spectra interpreted with the help of ^{26}Mg and D isotopic shifts and DFT (B3LYP/6-311+G*) calculations. Infrared absorptions at 772.9, 663.0, and 650.0 cm^{-1} are assigned to the X−Mg stretching modes of the $FMgCH_2$, $ClMgCH_2$, and $BrMgCH_2$ radicals, respectively. Bands at 502.2 and 2787.1 cm^{-1} are assigned to the Mg−C and C−H stretches of the $MgCH_2$ triplet carbene molecule.

The Mg−C stretching frequency of the metal carbene is of particular importance because it bears on the representation of metal-to-carbon bonding provided by the electronic structure calculations. Metal carbene complexes of iron and copper show metal−carbon stretching modes at 623.6 and 614.0 cm^{-1}, respectively. If the bonding in Mg and Be carbene systems were similar, one would expect the frequency of the metal−carbon

stretching mode for the magnesium carbene complex to be slightly higher owing to the lower mass of magnesium. However, the observed Mg−C stretching band is *significantly lower*, 502.2 cm^{-1}, indicating a much weaker metal−carbon bond than that found in the transition metal carbenes. These data are consistent with the bonding scheme described here.

Density functional calculations (B3LYP) on each of these species (and their beryllium analogues) reveal an unusual bonding interaction between the metal and carbon atoms. In contrast to well-known Fischer- and Schrock-type carbene complexes of transition metals, there is no significant π-bonding interaction in these species. For $BeCH_2$ and $MgCH_2$ species, the metal−carbon bond is a polar one-electron σ bond resulting from electron donation from metal to carbon in the β spin manifold. The insignificant π bonding that *does* exist between the metal and carbon atoms is a back-bonding interaction which is polarized in the opposite direction to that seen in Fischer carbenes and in metal−carbonyl complexes.

Addition of either hydrogen or halogen atoms to the metal increases the participation of the metal-centered p orbital in σ bonding and increases the bond strength, but does not induce significant participation from metal p-π (b_1) orbitals. The metal−carbon bonding orbital contains two electrons for the $HMCH_2$ and $XMCH_2$ carbenoid species. The meager π bonding is not discernibly different from that seen in the MCH_2 species.

While the B3LYP calculations generally predict frequencies and intensities in very good agreement with experiment, we find significant flaws in the DFT representation of the vibrational force fields in highly ionic molecules. In particular, the observed frequencies of C−H stretching modes are lower than predicted by calculation, and the coupling of the CH motion with other modes, the D-isotopic shifts, and absorption intensities of certain modes are underestimated. These disparities are also to be found in the DFT representation of spectra of $LiCH_3$, $NaCH_3$, and KCH_3. The description of the vibrational spectra for such systems can be improved by use of a better balanced basis set (improving the flexibility of the basis on the anionic site) and by more systematic treatment of correlation.

Acknowledgment. The authors acknowledge helpful discussions with G. P. Kushto and support from the National Science Foundation and the Petroleum Research Fund.

IC991229M